Laminar Mixed Convection in a Vertical Tube with a Longitudinal Rectangle Insert

Jun-Dar Chen* and Shou-Shing Hsieh†
National Sun Yat-Sen University, Kaohsiung, Taiwan 80424, Republic of China

The steady, fully developed laminar mixed convection in an axially uniformly heated vertical tube with an adiabatic rectangular insert is numerically studied systematically. Some cross-sectional flow and temperature patterns are provided for both upflow and downflow. Effects of heat-flux-to-mass-flow ratio, aspect ratio of insert, and the type of installation on the heat transfer and fluid friction characteristics and their net effect are determined. The buoyancy effect tends to make flow and temperature uniformly distributed in the cross section and to increase both friction factor and Nusselt number in the upflow; the opposite buoyancy effect occurs in the downflow.

Nomenclature

A_f = dimensionless flow area of the passage
D_h = dimensionless hydraulic diameter, d_h/R_o
d_h = hydraulic diameter, m
EH = horizontal eccentricity ratio, $e_h/R_o(1 - RR)$
EV = vertical eccentricity ratio, $e_v/R_o(1 - RR)$
e_h, e_v = horizontal and vertical eccentricities, m
f = friction factor, $2\tau/\rho w_m^2$
Gr = Grashof number, $g\beta q''_{in} d_h^4/(k\nu^2)$
g = gravitational acceleration, m/s^2
H = dimensionless height of insert, h/R_o
h = height of insert, m
k = thermal conductivity of fluid, W/m^2 − K
L = dimensionless width of insert, ι/R_o
N = dimensionless normal direction
Nu = Nusselt number of heated tube
P = dimensionless cross-sectionally mean pressure
PL = normalized peripheral position along insert, $\xi - \xi_{min}/\xi_{max} - \xi_{min}$
P_o = dimensionless perimeter of outer tube
Q_p = dimensionless overall heat transfer rate per unit pumping power
q''_{in} = prescribed averaged heat flux on outer tube, W/m^2
Re = Reynolds number, $w_m d_h/\nu$
RN = normalized radial distance
RR = radius ratio of circumscribed circle of insert to outer tube, $0.5(L^2 + H^2)^{0.5}$
R_o = radius of outer tube, m
T = dimensionless temperature
t = temperature, K
W = dimensionless axial velocity
w = axial velocity, m/s
X, Y, Z = dimensionless coordinates in physical domain
x, y, z = coordinates in physical domain, m
β = coefficient of thermal expansion of fluid, K^{-1}
θ = angular position, deg (Fig. 1)
ι = width of insert, m
ν = kinematic viscosity of fluid, m^2/s
ξ, η = dimensionless coordinates in transformed domain
τ = cross-sectionally averaged wall shear stress, N/m^2

Subscripts
b = bulk value
f = pure forced convection
m = mean value
max = maximum value
min = minimum value
s = surface value at outer tube
sr = value refer to outer tube at a reference location in the thermally developed region

Introduction

LAMINAR mixed convection in a vertical channel is important in many recent technological applications, e.g., solar collector systems, compact cooling of electronic equipment, heat exchangers, and certain types of catalytic devices. Generally, heat transfer in these devices is by turbulent convection, but laminar convection and associated buoyancy effects are of considerable interest at low flow conditions or during shutdown. It is well recognized that the heat transfer of mixed convection can be significantly different from that of both forced and free convections. The studies of mixed convection in vertical ducts had recently been reviewed.[1,2] For singly connected ducts, configurations of tube and channel of two parallel plates were commonly considered. However, for vertical doubly connected ducts, only the configurations of concentric tube annuli had been presented in the open literature. An experimental investigation of combined free and forced convection in an internally heated concentric tube annulus in inclined positions was reported by Bohne and Obermeier.[3] The influence of inclination and flow direction as determined for a large range of Reynolds and Rayleigh numbers. For mixed convection of water in vertical concentric tube annuli, El-Genk and Rao[4] provided general correlations of hydrodynamically developed but thermally developing flow at low Reynolds numbers for upflow and/or downflow and natural flow, and performed both flow visualization and heat transfer measurements to investigate buoyancy-induced instability of developing laminar upflow and downflow.[5]

To compute laminar mixed convection in a vertical duct, most efforts used the boundary-layer theory formulation and/or involved the fully developed assumption.[6-11] Although good agreements were reported between the theoretical predictions and the experimental data at low heat-flux-to-mass-flow ratios (Gr/Re), at higher Gr/Re values, theoretical predictions were

Received Aug. 23, 1990; revision received Jan. 22, 1991; accepted for publication Jan. 25, 1991. Copyright © 1991 by the American Institute of Aeronautics and Astronautics, Inc. All rights reserved.

*Graduate Student, Department of Mechanical Engineering.
†Professor and Chairman, Department of Mechanical Engineering. Member AIAA.

consistently lower than experimental data because the variations of density and viscosity will induce hydrodynamic instability, causing a disturbance that grows as it is convected downstream and initiating transition from stable laminar flow to tubulent flow.[12] Sherwin[13] estimated the minimum *Gr/Re* values required to initiate transition in vertical concentric tube annuli using the fully developed flow approximation, and suggested that the practical minimum *Gr/Re* value should be twice that of the prediction. Accounting for the hydrodynamic instability, Yao and Rogers[14] analyzed the mixed convection in a vertical tube annulus with an outer-to-inner-radius ratio of 100, and showed that steady parallel mixed convection with reversed flow regions is unlikely to be experimentally observed except at extremely small Reynolds number. Rao and El-Genk[15] developed a prediction model to determine the location of incipient instability. Results showed that neglecting the radial momentum can underpredict the location of incipient instability, but neglecting the axial momentum diffusion only insignificantly affects that location. In contrast, little is known about the mixed convection in vertical noncircular annuli.

As one of the practically used displaceable heat transfer augmentation devices, longitudinal rectangular inserts are found inserted in the tubes of tubular heat exchangers to enhance tubeside heat transfer. The physical configuration is depicted in Fig. 1, which forms a typical example of noncircular annulus. Fully developed laminar forced convection in such a configuration had been numerically analyzed by the authors[16,17] using the boundary-fitted coordinate system (BFCS) to tackle the irregular configuration. This paper concerns the buoyancy effect on the fully developed laminar forced convection for both upflow and downflow in the same configuration. Rectangular inserts of aspect ratios (width to height, *L/H*) of 1 (square) and 5 (thin plate) are considered. To place the emphasis on buoyancy effect, the inserts are chosen that have a radius ratio of circumscribed circle of insert to outer tube of 0.5. In addition to the concentric installation, vertically and horizontally eccentric installations of the insert are also taken into account to determine their influences on the mixed convection.

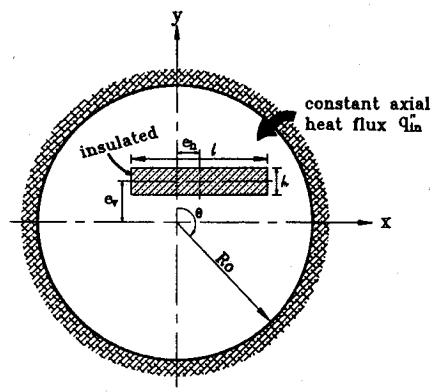

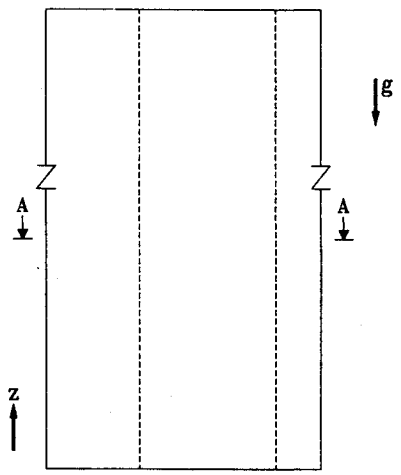

Fig. 1 Noncircular annular duct.

Theoretical Analysis

Consider the steady, fully developed laminar flow in an axially uniformly heated vertical tube with a longitudinal rectangular insert (Fig. 1). Fluid properties are assumed constant except the density, of which variation with temperature is treated via Boussinesq approximation. Since the tube is made of metal for practical application, it is reasonable to assume that the tube, in addition to being axially uniformly heated, has a peripherally constant wall temperature, t_s, rather than a uniform heat flux.[17] Due to axially uniform heating on the outer tube, the z (axial) directional rising rate of fluid temperature becomes constant and is equal to $\alpha q''_{in} P_o/(k w_m R_o A_f)$. For fully developed flow, the dimensionless axial momentum and energy conservation equations are formulated as

$$\frac{\partial^2 W}{\partial X^2} + \frac{\partial^2 W}{\partial Y^2} - \frac{dP}{dZ} + \frac{Gr}{Re}\frac{T}{D_h^3} = 0 \tag{1}$$

$$\frac{\partial^2 T}{\partial X^2} + \frac{\partial^2 T}{\partial Y^2} - W\frac{P_o}{A_f} = 0 \tag{2}$$

In the above equation, the x, y coordinates are made dimensionless by R_o, the z coordinate by $R_o Re/D_h$, the axial velocity by w_m, and the cross-sectionally mean pressure by ρw_m^2. The temperature relative to the constant outer tube temperature is nondimensionalized by $q''_{in} R_o/k$. The parameters appearing in the equations are the Reynolds number *Re* and the Grashof number *Gr*. Because of the definition of dimensionless groups, their ratio, *Gr/Re* (heat-flux-to-mass-flow ratio), instead of the conventional Gr/Re^2 (ratio of buoyant to viscous forces), appears in the last term of the left hand side of Eq. (1). Positive *Gr/Re* stands for upflow and negative *Gr/Re* for downflow. The cross-sectionally mean pressure in Eq. (1) is a modified one that is the thermodynamic cross-sectionally mean pressure plus the quantity $\rho_{sr} g(z - \beta a z^2/2)$, with z measured from a reference axial location in the thermally developed region and ρ_{sr} the fluid density at that location. The boundary conditions are expressed as

$$W = 0; \quad \frac{\partial T}{\partial N} = 0 \quad \text{at insert} \tag{3a}$$

$$W = 0; \quad T = 0 \quad \text{at outer tube} \tag{3b}$$

The axial gradient of cross-sectionally mean pressure, dP/dZ, can be determined with the use of global mass conservation

$$\iint W dX dY = A_f \tag{4}$$

To tackle the irregular flow configuration (Fig. 1), Eqs. (1–4) are first tranformed to the BFCS, discretized by the finite volume discretization method, and calculated by a line-by-line iterative procedure with the SLOR method. The overrelaxation factor for each variable is chosen as 1.7 in the present study. A nonorthogonal 73 × 36 grid, with nodes equi-spaced along and grid line more closely packed near both walls, is numerically generated by the elliptic generation method[18] for computation. The dP/dZ term is calculated numerically by the method of Patankar and Spalding.[19] In each run, the iteration procedure is terminated when $|(\phi^{n+1} -$

$\phi^n)/\phi^{n+1}| \leq 10^{-5}$ for $\phi = W$ and T at each node. The friction factor-Reynolds number product fRe is expressed in terms of dimensionless variables as

$$fRe = \frac{D_h^2}{2}\left(-\frac{dP}{dZ}\right) \tag{5}$$

and the local and peripherally averaged Nusselt numbers are expressed in dimensionless form as[17]

$$Nu = \left(\frac{\partial T}{\partial N}\right)_s D_h/T_b; \qquad Nu_m = -D_h/T_b \tag{6}$$

Results and Discussion

As mentioned above, the emphasis of this work is on the buoyancy effect on the fully developed laminar forced convection. To avoid the possible occurrences of flow reversal and transition that cannot be properly treated by the present mathematic model[5,14,15] and to assure the accuracy of results, numerical solutions are obtained for low Gr/Re values ranging from -100 to 100. As typical representations, results of square and thin-plate inserts of concentric installation and horizontally and vertically eccentric installations with eccentricity ratio of 0.5 are presented. To check the accuracy of the computed results, computations were first carried out for fully developed laminar mixed convection in a vertical tube annulus of asymmetric wall temperatures with the outer tube having a high temperature, corresponding to the case of Kuo and Lin,[6] for inner-to-outer-radius ratio of 0.5. Figure 2 presents the calculated axial gradients of pressure for various Gr/Re values. These results are found to be in excellent agreement with those provided by analytical solutions.[6] Furthermore, the calculated axial velocity profiles for cases of $Gr/Re = -100$ and 100 are shown in Fig. 3, which agrees well with the analytical ones.[6] Computations were also performed for fully developed laminar mixed convection in a vertical tube annulus with axially uniform heating at outer tube and insulating at inner tube. The calculated Nu/Nu_f values of the heated tube

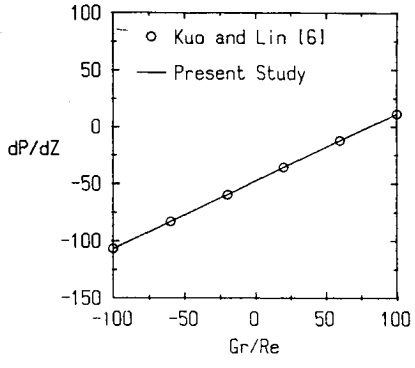

Fig. 2 Axial gradient of cross-sectionally mean pressure of a concentric tube annulus.

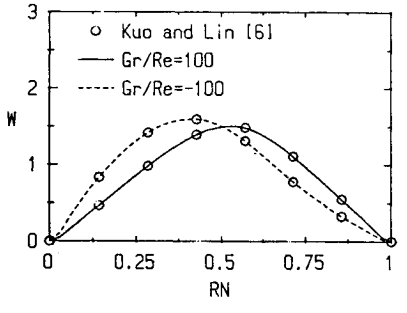

Fig. 3 Radial distribution of axial velocity of a concentric tube annulus.

Table 1 Buoyancy effect on the Nusselt numbers of a concentric tube annulus

	Gr/Re					
Nu/Nu_f	1750	350	3.5	0	−3.5	−350
Present study	1.485	1.119	1.001	1.0	0.999	0.869
Kim[7,8]	1.485	1.118	1.002	1.0	0.998	0.870

are compared with those provided analytically by Kim[7,8] in Table 1 with an inner-to-outer-radius ratio of 0.4. It is found that the present study reproduces well the analytical solutions. Although no results of laminar mixed convection in eccentric tube annuli or concentric and/or eccentric noncircular annuli are available in the literature, calculations were carried out for laminar forced convection (a special case of mixed convection of $Gr/Re = 0$) instead in eccentric tube annuli and in noncircular annuli of tubes with concentric inner square cores. The comparisons showed that the results have an accuracy of the order of 1%.[17] Furthermore, a finer 97 × 44 grid was used in some cases to check the grid dependence of the calculated results. The deviations were found to be within ±0.5%. In view of these validations, the present solution procedure and employed grid layout are adequate to obtain accurate results for practical purposes.

The flow and temperature patterns are presented by isotherms and isovels in the cross section. Figures 4 and 5 show these patterns for square insert and thin-plate insert, respectively. For square insert, it is obvious that vertically and horizontally eccentric installations have the same patterns; thus, only those of vertically eccentric installation are presented.

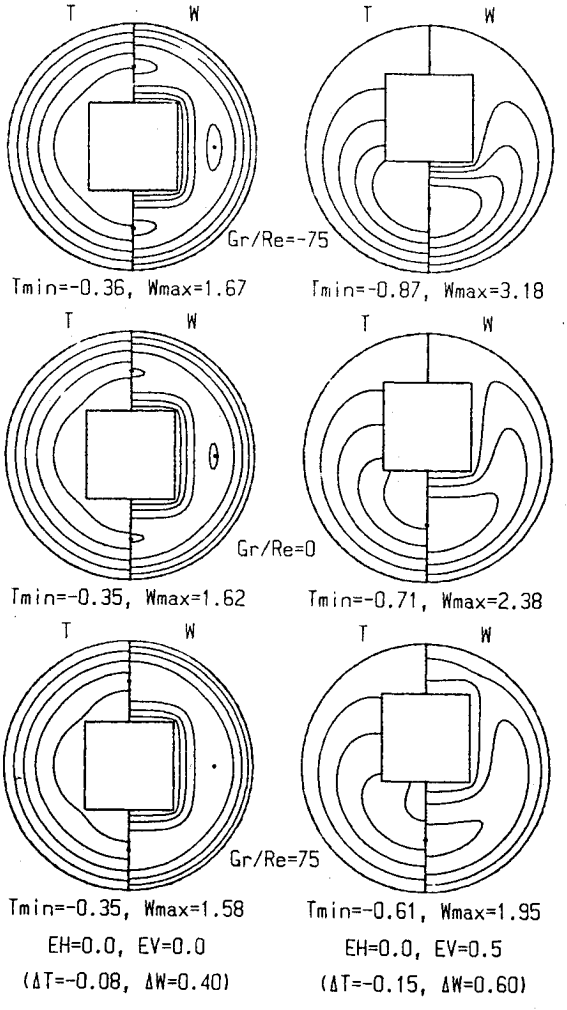

Fig. 4 Isovels and isotherms in the cross section of a vertical tube with a square insert.

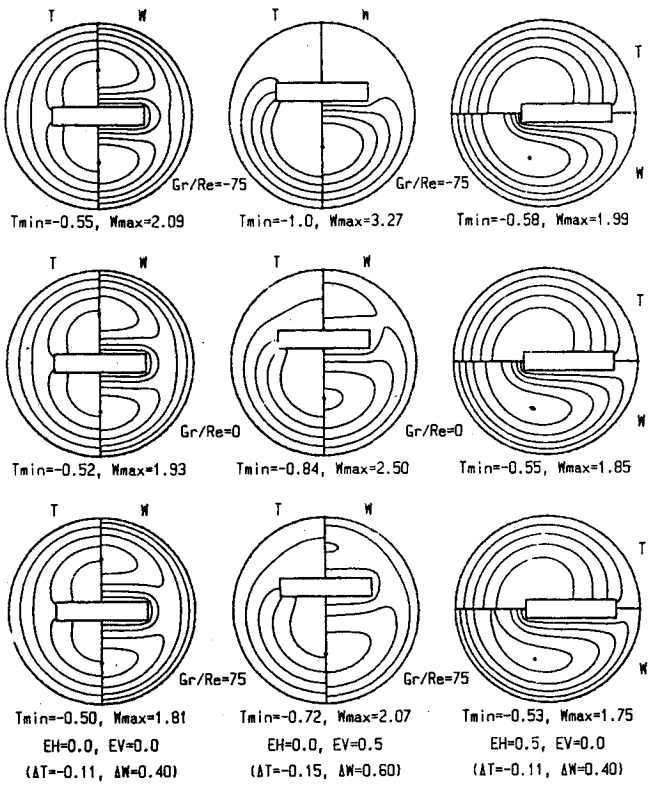

Fig. 5 Isovels and isotherms in the cross section of a vertical tube with a thin-plate insert.

However, these patterns of thin-plate insert vary with the type of eccentric installation; those of both eccentric installations are provided separately. Because of the symmetric nature, the isotherms are plotted in the left half and isovels in the right half of the cross section for concentric and vertically eccentric installations; for horizontally eccentric installation, however, the isotherms are plotted in the upper half and isovels in the lower half. The W_{max} and T_{min} (a measure of the uniformity of cross-sectional temperature distribution) values are listed below the annuli for reference and the dot denotes the position of W_{max} value. These contours are equispaced with interval values also listed below the annuli. Note that by the imposed thermal conditions, the maximum fluid temperature occurs at the outer tube with a value of zero by the definition of nondimensional temperature. The interior fluid temperatures are all negative accordingly.

Figures 4 and 5 reveal that the buoyancy effect tends to decrease the W_{max} and absolute T_{min} values in the upflow, but the opposite trend occurs in the downflow for each insert despite the type of installation. Although the cross-sectional distribution of flow rate is solely dependent on that of gap clearance in forced convection,[16,17] in the upflow, buoyancy effect causes the velocity (flow rate) to increase and the fluid temperature to decrease in regions of small gap clearance, but the opposite effect occurs in regions of large gap clearance. This implies that the buoyancy effect makes the cross-sectional distributions of flow rate and fluid temperature uniform. In the downflow, the buoyancy effect is opposite that in the upflow. For square insert, the buoyancy effect becomes evident in both eccentric installations. For thin-plate insert, although the buoyancy effect is significant in a vertically eccentric installation, in concentric and horizontally eccentric installations it is only slight. At the same *Gr/Re* value, square insert has more uniform cross-sectional distributions of velocity (flow rate) and fluid temperature than thin-plate inset in all installations studied except a horizontally eccentric one.

For each insert in each installation studied, a close examination of Figs. 4 and 5 reveals that fluid temperature near the outer tube is slightly affected by the buoyancy effect. In downflow, Fig. 4 shows that, for the square insert, fluid temperature near the insert decreases in a concentric installation. In a vertically eccentric installation, fluid temperature near the insert increases at the lower part, but decreases at the upper part, of the cross section in accordance with the flow rate redistribution. For the thin-plate insert, Fig. 5 shows that, in concentric and horizontally eccentric installations, a significant temperature decrease of fluid near the insert can be observed only at angular locations with large gap clearance. However, fluid temperature near the insert increases at a location with small gap clearance and decreases at a location with large gap clearance in a vertically eccentric installation. The opposite buoyancy effect on the temperature pattern is observed in upflow.

To interpret the buoyancy effect more clearly, radial distributions of dimensionless axial velocity of both inserts at some angular locations are provided in Figs. 6 and 7 in which a symbol *RN* is used to present the normalized (with respect to the gap clearance) radial distance relative to the insert at each angular locations with $RN = 0$ at insert and $RN = 1$ at tube. Obviously, at these locations, the *RN* can be mathematically expressed as follows:

$$RN = \frac{\eta - \eta_{min}}{\eta_{max} - \eta_{min}} \tag{7}$$

In downflow, Figs. 6 and 7 show that, for each insert, the buoyancy-induced natural convection decelerates velocities near the tube at each angular location despite of the type of installation. However, those near the insert obviously depend on the angular location, insert type, and the type of installation. Except for the case of a square insert in a horizontally eccentric installation, the buoyancy effect decelerates the fluids near the insert at locations with small gap clearance, but accelerates those at locations with large gap clearance. This is because the fluids at locations of small gap clearance have low kinetic energy in forced convection, and can hardly overcome the additional flow resistance by buoyant force, thus they are further decelerated. Because of the constraint of constant cross-sectional mass flow, velocities at locations of large gap clearance must eventually increase. For the concentrically installed square insert, due to slight angular variation of gap clearance and flow rate, buoyant force acts nearly

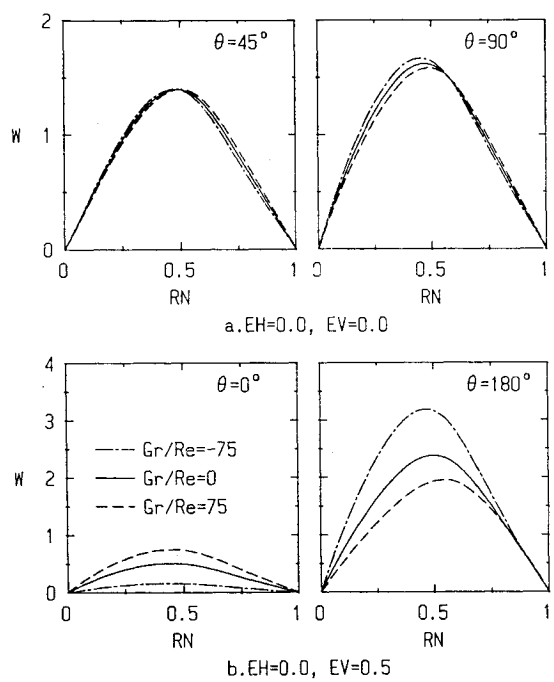

Fig. 6 Radial distribution of axial velocity at some angular locations in a vertical tube with a square insert.

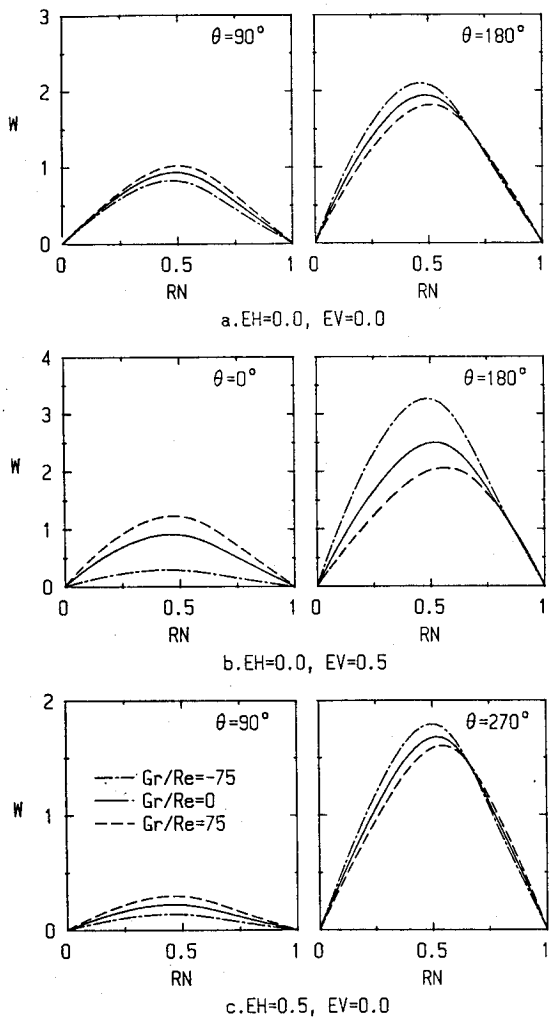

Fig. 7 Radial distribution of axial velocity at some angular locations in a vertial tube with a thin-plate insert.

equally to each angular location. Because of the increase of velocities near the tube and the constraint of constant cross-sectional mass flow, velocities near the insert increase and the velocity peak shifts toward the insert at each angular location. Obviously, the opposite buoyancy effect appears in upflow. Generally speaking, under the same heat-flux-to-mass-flow ratio, the downflow is more sensitive to the buoyancy effect than the upflow.

It has been indicated that the angular distributions of the local Nusselt number, Nu, of the tube and the wall temperature, T_{in}, of the insert are proportional and inversely proportional, respectively, to the distribution of gap clearance in forced convection.[16,17] Owing to the buoyancy-induced velocity change at each angular location, it is of practical interest to investigate the accompanied influence on both Nu and T_{in} values.

For all installations studied, Figs. 8 and 9 show the angular variation of T_{in} for the square insert and thin-plate insert, respectively. The PL in these figures denotes the normalized (w.r.t. insert perimeter) peripheral position along the insert measured from the midpoint of the upper side of the insert. A comparison of the change of T_{in} with that of velocity shows that the T_{in} change is inversely proportional to the velocity change near the insert. In upflow, because the buoyancy effect decreases the velocities near the insert for a square insert in a concentric installation, it always raises T_{in} at each angular location. In the case of a square insert in a vertically eccentric installation, the buoyancy effect only raises T_{in} at the lower part of the cross section ($0.25 \leq PL \leq 0.75$) where velocities near the insert decrease. It is obvious that a horizontally eccentric installation has the same buoyancy effect on T_{in} as a vertically eccentric one with a PL shift of 0.25. For a thin-plate insert in concentric and horizontally eccentric installations, the buoyancy effect generally raises T_{in} with significant change at locations of large gap clearance. Both inserts have a similar buoyancy effect on T_{in} in a vertically eccentric installation. In general, for each insert in each installation, the buoyancy effect tends to make the angular variation of T_{in} uniform. In downflow, the opposite trend is observed.

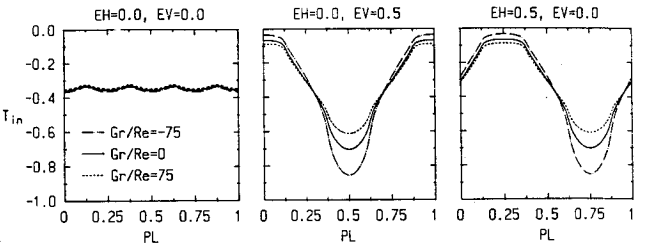

Fig. 8 Angular variation of inner wall temperature in a vertical tube with a square insert.

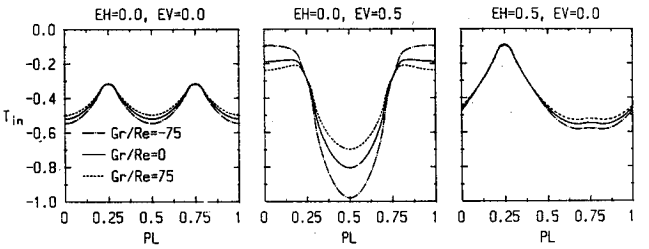

Fig. 9 Angular variation of inner wall temperature in a vertical tube with a thin-plate insert.

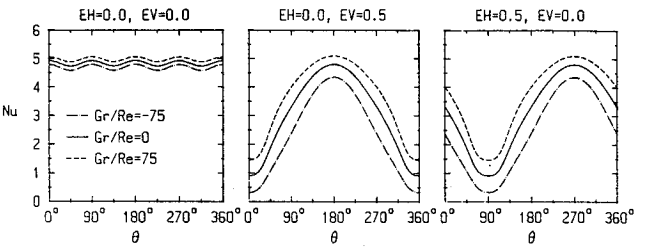

Fig. 10 Angular variation of local Nusselt number in a vertical tube with a square insert.

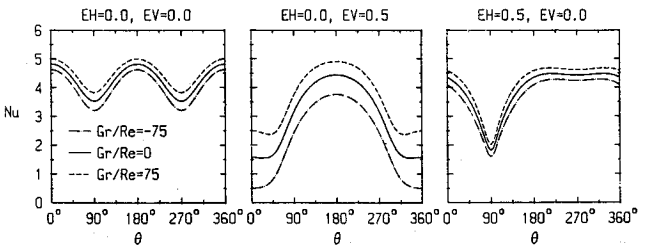

Fig. 11 Angular variation of local Nusselt number in a vertical tube with a thin-plate insert.

The angular variation of Nu value of three installations is presented in Fig. 10 for a square insert and in Fig. 11 for a thin-plate insert. A close inspection of these figures reveals that the buoyancy effect alters the magnitude appreciably, but changes the angular variation of the Nu value only slightly for each insert in each installation. The heat transfer is enhanced in upflow and, on the other hand, downgraded in downflow by the buoyancy effect. According to the definition of local Nusselt number, fluid temperature near the tube is found to be decreased in upflow but increased in downflow by the buoyancy effect. Due to the aforementioned finding that the buoyancy effect always increases in upflow and decreases in downflow the velocities (flow rate) near the tube

Table 2 Overall Nusselt numbers and *fRe* factors

		$EH = 0, EV = 0$			$EH = 0, EV = 0.5$			$EH = 0.5, EV = 0$		
Gr/Re	L/H	fRe	Nu_m	Q_p	fRe	Nu_m	Q_p	fRe	Nu_m	Q_p
100	1	33.25	5.042	1.026	33.11	3.814	0.777	33.11	3.814	0.777
	5	32.92	4.582	0.919	33.05	3.813	0.764	31.75	4.225	0.857
50	1	28.25	4.948	1.063	26.27	3.486	0.767	26.27	3.486	0.767
	5	27.37	4.429	0.944	26.17	3.440	0.745	25.73	4.073	0.887
0	1	23.15	4.853	1.114	18.69	3.102	0.765	18.69	3.102	0.765
	5	21.63	4.269	0.984	18.41	3.004	0.731	19.47	3.915	0.935
−50	1	17.94	4.757	1.189	9.990	2.644	0.803	9.990	2.644	0.803
	5	15.65	4.101	1.054	9.315	2.494	0.762	12.95	3.750	1.026
−100	1	12.63	4.658	1.308	—	—	—	—	—	—
	5	9.426	3.925	1.194	—	—	—	6.131	3.577	1.256

Table 3 Coefficients of correlation of Nu_m value

EH	EV	L/H	$B_1 \times 10^3$	$B_2 \times 10^6$	Maximum error (%)	Gr/Re
0.0	0.0	1	0.395	−0.050	0.014	−100–100
		5	0.769	−0.369	0.010	−100–100
0.5	0.0	1	2.741	−4.657	0.163	−75–100
		5	0.827	−0.347	0.022	−100–100
0.0	0.5	1	2.741	−4.657	0.163	−75–100
		5	3.165	−4.838	0.096	−75–100

Table 4 Coefficients of correlation of *fRe* factor

EH	EV	L/H	$C_1 \times 10^3$	$C_2 \times 10^6$	Maximum error (%)	Gr/Re
0.0	0.0	1	4.453	−0.922	0.016	−100–100
		5	5.427	−2.138	0.050	−100–100
0.5	0.0	1	8.824	−11.80	1.290	−75–100
		5	6.574	−2.694	0.258	−100–100
0.0	0.5	1	8.824	−11.80	1.290	−75–100
		5	9.298	−14.35	2.190	−75–100

for each insert in each installation, it can be inferred that the change of Nu is proportional to that of flow rate near the tube.

To provide useful information for practical applications, Table 2 summarizes the calculated averaged Nusselt number and friction factor (in terms of fRe) of both inserts in concentric and/or eccentric installations. Furthermore, correlations of Nu_m values and fRe factors are provided via the least squares method of the following forms

$$\frac{Nu_m}{(Nu_m)_f} = 1 + B_1 \frac{Gr}{Re} + B_2 \left(\frac{Gr}{Re}\right)^2 \tag{8}$$

$$\frac{fRe}{(fRe)_f} = 1 + C_1 \frac{Gr}{Re} + C_2 \left(\frac{Gr}{Re}\right)^2 \tag{9}$$

to facilitate the extrapolation of the results. Tables 3 and 4 list the values of B_1, B_2, C_1, C_2, the maximum errors, and the valid ranges of Gr/Re value of both inserts in all the installations studied. As can be seen from Table 2, both Nu_m value and fRe factor vary with the Gr/Re value; it is, therefore, of practical interest to assess the buoyancy effect on the net effect between heat transfer augmentation and pumping power increase. A dimensionless overall heat transfer rate per unit pumping power, Q_p, is used to measure the net effect and is defined as[17]

$$Q_p = -\left(\frac{0.4972}{T_b}\right)\left(\frac{D_h^2 A_f}{fRe}\right) \tag{10}$$

The Q_p value of each case is also listed in Table 2. However, since negative fRe factors (positive or adverse axial gradient of pressure) suggesting possible flow separation at the walls are obtained at some Gr/Re values, no result in these cases is provided in Table 2 because the present model cannot properly treat these cases as mentioned previously. Note that the downflow is more prone to the possible flow separation than the upflow, because in the former the buoyant force forms additional flow resistance.

For each insert, a close examination of Table 2 reveals that, despite of the type of installation, the buoyancy effect increases in upflow but decreases in downflow both fRe factor and Nu_m value. The changing rates of these values in downflow are faster than those in upflow, which implies that the buoyant force distorts the velocity and temperature distributions more severely in downflow than in upflow. The square insert has a higher fRe factor and Nu_m value than the thin-plate insert in concentric and vertically eccentric installations. Also revealed in Table 2 is that, in downflow, the buoyancy effect increases the Q_p value for each insert in each installation studied. However, the buoyancy effect on Q_p in upflow shows dependence on the types of installation and insert. For a square insert in upflow, while the buoyancy effect decreases the Q_p value in the concentric installation, such effect increases the Q_p value in both eccentric installations. For a thin-plate insert in upflow, the Q_p value is decreased by the buoyancy effect in all installations studied except the vertically eccentric one in which the opposite trend is observed. However, in all installations studied except the horizontally eccentric one, the square insert has a higher Q_p value than the thin-plate insert in the range of Gr/Re value studied. This implies that the condition of superiority of a square insert as a tubeside heat-transfer augmentative device to a thin-plate insert provided in forced convection[17] even though the buoyancy effect is present.

Conclusion

A numerical study for the steady, fully developed laminar mixed convection in an axially uniformly heated vertical tube with an adiabatic rectangular longitudinal insert is presented in this paper. The cross-sectional flow and temperature patterns are calculated for a range of heat-flux-to-mass-flow ratio, two aspect ratios of rectangular insert, and three installations of insert in upflow and downflow. The buoyancy effect on the heat transfer and fluid friction characteristics and their net effect is also determined. The following conclusions can be drawn based on the results:

1) When the buoyancy effect is present, cross-sectional distributions of flow rate and fluid temperature are not solely dependent on that of gap clearance for each insert in each installation. In upflow, the buoyancy effect tends to distribute uniformly the flow rate and fluid temperature in the cross section, which becomes more evident in an eccentric installation than in a concentric one. Although the buoyancy effect increases the flow rate near the tube, the influence on the flow rate near the insert depends on the type of insert, type of installation, and angular location. In downflow, the opposite buoyancy effect to that in upflow is observed. The cross-sectional distribution of fluid temperature is inversely proportional to that of flow rate in both upflow and downflow.

2) In both upflow and downflow, for each insert the buoyancy effect alters the magnitude appreciably but the angular variation of the local Nusselt number only slightly, and affects significantly the wall temperature of the insert only at locations of large gap clearance. The change of wall temperature of the insert is inversely proportional to that of flow rate near the insert, but the change of local Nusselt number is proportional to that of flow rate near the tube. Under the same heat-flux-to-mass-flow ratio, the buoyancy effect is more evident in downflow than in upflow.

3) For each installation of each insert, the buoyancy effect increases in upflow but decreases in downflow the fRe factor and Nu_m value. While the net effect is increased by the buoyancy effect in downflow, the buoyancy effect on the net effect in upflow depends on the type of installation and insert. Generally speaking, in the range of Gr/Re values studied, the square insert has a higher fRe factor and Nu_m value, and better net effect than the thin-plate insert in all installations studied except the horizontally eccentric one.

References

[1]Jackson, J. D., Cotton, M. A., and Axcell, B. P., "Studies and Mixed Convection in Vertical Tubes," *International Journal of Heat and Fluid Flow*, Vol. 10, 1989, pp. 2–15.

[2]Kakac, S., Shah, R. K., and Aung, W. (ed.), *Handbook of Single-Phase Convection Heat Transfer*, 1st ed., Wiley, New York, 1987, Chap. 15.

[3]Bohne, D., and Obermeier, E., "Combined Free and Forced Convection in a Vertical and Inclined Cylindrical Annulus," *8th International Heat Transfer Conference*, San Francisco, 1986, pp. 1401–1406.

[4]El-Genk, M. S., and Rao, D. V., "Heat Transfer Experiments and Correlations for Low-Reynolds-Number Flows of Water in Vertical Annuli." *Heat Transfer Engineering*, Vol. 10, 1989, pp. 44–57.

[5]El-Genk, M. S., and Rao, D. V., "Buoyancy Induced Instability of Laminar Flows in Vertical Annuli: I. Flow Visualization and Heat Transfer Experiments," *International Journal of Heat and Mass Transfer*, Vol. 33, 1990, pp. 2145–2159.

[6]Kuo, H. S., and Lin, S. W., "Fully Developed Laminar Mixed Convection in a Vertical Annular Duct with Asymmetric Wall Temperatures," *5th National Conference on Mechanical Engineering*, Chinese Society of Mechanical Engineering, Taipei, Dec. 1988, pp. 569–576.

[7]Kim, J. H., "Analysis of Laminar Mixed Convection in Vertical Tube Annulus with Upward Flow," ASME-HTD-42, 1985, pp. 91–98.

[8]Kim, J. H., "Analysis of Laminar Natural Convection Superimposed on Downward Flow in Vertical Tube Annulus," *ASME Paper 85-WA/HT-13*, 1985.

[9]Hashimoto, K., Akino, N., and Kawamura, H., "Combined Forced-Free Laminar Heat Transfer to a Highly Heated Gas in a Vertical Annulus," *International Journal of Heat and Mass Transfer*, Vol. 29, 1986, pp. 145–151.

[10]Aung, W., and Worku, G., "Developing Flow and Flow Reversal in a Vertical Channel with Asymmetric Wall Temperatures," *ASME Journal of Heat Transfer*, Vol. 108, 1986, pp. 299–304.

[11]El-Shaarawi, M. A. I., and Sarhan, A., "Free Convection Effects on the Developing Laminar Flow in Vertical Concentric Annuli," *ASME Journal of Heat Transfer*, Vol. 102, 1980, pp. 617–622.

[12]Gebhart, B., and Mahajan, R. L., "Instability and Transition in Buoyancy-Induced Flows," *Advances in Applied Mechanics*, Vol. 22, 1982, pp. 231–315.

[13]Sherwin, K., "Combined Natural and Forced Laminar Flow in Vertical Annuli," *British Chemical Engineering*, Vol. 14, 1969, pp. 1215–1217.

[14]Yao, L. S., and Rogers, B. B., "Mixed Convection in an Annulus of Large Aspect Ratio," *ASME Journal of Heat Tranfer*, Vol. 111, 1989, pp. 683–689.

[15]Rao, D. V., and El-Genk, M. S., "Buoyancy Induced Instability of Laminar Flows in Vertical Annuli: II. Model Development and Analysis," *International Journal of Heat and Mass Transfer*, Vol. 33, 1990, pp. 2161–2172.

[16]Chen, J. D., and Hsieh, S. S., "Laminar Forced Convection in Circular Tube Inserted with a Longitudinal Rectangular Plate." *Journal of Thermophysics and Heat Transfer*, in press.

[17]Chen, J. D., and Hsieh, S. S., "Assessment Study of Longitudinal Rectangular Plate Inserts as Tubeside Heat Transfer Augmentative Devices," *International Journal of Heat and Mass Transfer*.

[18]Thompson, J. F., Thames, F. C., and Mastin, C. W., "TOMCAT—a Code for Numerical Generation of Boundary Fitted Curvilinear Coordinate Systems of Fields Containing Any Number of Arbitrary 2-D Bodies," *Journal of Computational Physics*, Vol. 24, 1977, pp. 274–302.

[19]Patankar, S. V., and Spalding, D. B., "A Calculation Procedure for Heat, Mass and Momentum Transfer in Three-Dimensional Parabolic Flows," *International Journal of Heat and Mass Transfer*, Vol. 15, 1972, pp. 1187–1806.